Macromolecules

ARTICLE

pubs.acs.org/Macromolecules

Controlling the Self-Assembly of Binary Copolymer Mixtures in Solution through Molecular Architecture

Martin J. Greenall,[†] Peter Schuetz,[*,‡] Steve Furzeland,[‡] Derek Atkins, D. Martin A. Buzza,[§] Michael F. Butler,[‡] and Tom C. B. McLeish[⊥]

[†]Institut Charles Sadron, 23, rue du Loess, 67034 Strasbourg, France

[‡]Unilever R&D Colworth, Colworth Park, Sharnbrook, MK44 1LQ, U.K.

[§]Department of Physics, The University of Hull, Cottingham Road, Hull HU6 7RX, U.K.

[⊥]Department of Physics, Durham University, South Road, Durham DH1 3LE, U.K.

ABSTRACT: We present a combined experimental and theoretical study on the role of copolymer architecture in the self-assembly of binary PEO−PCL mixtures in water−THF and show that altering the chain geometry and composition of the copolymers can control the form of the self-assembled structures and lead to the formation of novel aggregates. First, using transmission electron microscopy and turbidity measurements, we study a mixture of sphere-forming and lamella-forming PEO−PCL copolymers and show that increasing the molecular weight of the lamella-former at a constant ratio of its hydrophilic and hydrophobic components leads to the formation of highly curved structures even at low sphere-former concentrations. This result is explained using a simple argument based on the effective volumes of the two sections of the diblock and is reproduced in a coarse-grained mean-field model: self-consistent field theory (SCFT). Using further SCFT calculations, we study the distribution of the two copolymer species within the individual aggregates and discuss how this affects the self-assembled structures. We also investigate a binary mixture of lamella-formers of different molecular weights and find that this system forms vesicles with a wall thickness intermediate to those of the vesicles formed by the two copolymers individually. This result is also reproduced using SCFT. Finally, a mixture of sphere-former and a copolymer with a large hydrophobic block is shown to form a range of structures, including novel elongated vesicles.

INTRODUCTION

Amphiphiles such as block copolymers and lipids can self-assemble into many different structures when dissolved in solution.[1,2] The case of block copolymers has proved especially interesting to researchers in recent years, for a variety of reasons.[3] First, the study of block copolymers is a promising route to a fundamental model of the self-assembly of amphiphiles in solution, since the theoretical understanding of the constituent polymer molecules is on a firm footing. Well-established methods such as self-consistent field theory (SCFT)[4−6] have provided considerable insight into the self-assembly of polymers, especially in melts,[7,8] while using simple models of the individual polymer molecules. Second, vesicles formed from block copolymers show more promise as vehicles for drug delivery[9] than similar structures formed from lipids, as the thickness and low solubility of their membranes means that they can be longer-lived and less permeable.[10,11]

For solutions of a single type of diblock copolymer, it is often relatively straightforward to understand why a given type of aggregate forms in a given system. The main factor that determines the shape of the structures is the architecture of the copolymer, that is, the size of its hydrophilic and hydrophobic blocks[12] (although other factors, such as the overall size of the copolymer, may also play a role[13]). If the hydrophilic component is large compared to the hydrophobic component, then curved aggregates such as spherical or cylindrical micelles form. Conversely, if the hydrophobic component is large, lamellar structures such as vesicles are observed.[12] Recently, we demonstrated this behavior in a study of PCL-*b*-PEO block copolymers with various volume fractions of the hydrophobic block (PCL).[14] Here, large volume fractions f_{EO} of the hydrophilic block (PEO) resulted in micelles ($f_{EO} > 0.3$), lower f_{EO} favored wormlike micelles ($0.25 < f_{EO} < 0.3$), and still lower fractions ($f_{EO} < 0.25$) led to the formation of vesicles.

We can gain increased control over the self-assembly by mixing two types of amphiphiles that individually form aggregates of different curvatures. Such mixtures are well-known in cell biology, where different lipids can be sorted by segregation to regions of high and low curvature,[15,16] and have also been studied in the context of lipid−detergent systems.[17,18] More recently, they have been investigated in block copolymer solutions. For example, Jain and Bates[2] have studied mixtures of poly(ethylene oxide)−polybutadiene (PEO−PB) and have found that blending ratio can be used to control self-assembly and furthermore that novel structures such as undulating cylinders form. They also found that different aggregates form depending on whether the

Received: April 13, 2011
Revised: June 6, 2011
Published: June 16, 2011

Table 1. Polymers Used in This Study, with Their Properties from Light Scattering

commercial sample code	sample formula	M_w[a]	M_w/M_n	f_{EO}[b]	morphology[c]	R_h (nm)[d]
$PCL_{10K}PEO_{2K}$	PEO_{45}-*b*-PCL_{101}	17300	1.36	0.15	V	220
$PCL_{5K}PEO_{1K}$	PEO_{23}-PCL_{47}	7100	1.15	0.17	V	170
$PCL_{5K}PEO_{2K}$	PEO_{45}-*b*-PCL_{43}	7800	1.16	0.3	C, S	30
$PCL_{5K}PEO_{550}$	PEO_{12}-*b*-PCL_{56}	6380	1.15	0.08	P	n/a

[a] Total molecular weight from GPC (PEO standards). [b] Volume fraction of the EO block calculated from the melt densities of the two blocks. [c] Morphology determined by light scattering and cryo-TEM (S = spherical micelles, C = wormlike micelle, V = vesicle, P = precipitate; in the cases of mixed morphologies the majority component is written first). [d] Hydrodynamic radius from dynamic light scattering (DLS) after dialysis.

two polymer species are mixed before or after their individual self-assembly.[2]

In a recent study of a mixture of sphere-forming and lamella-forming polycaprolactone-*co*-poly(ethylene oxide) in water−THF mixed solvents,[19] we have built on this work by controlling the quantities of water and THF to mix sphere- and lamella-forming copolymers not only before and after but also during their individual self-assembly. Those copolymers mixed before self-assembly (premixed) formed a sequence of aggregates of increasing curvature as the amount of sphere-former was increased, forming vesicles, then a mixtures of vesicles, rings, and worms, and finally spherical micelles. This series of shape transitions has also been observed in lipid−detergent mixtures[17,18] and has been studied theoretically using self-consistent field theory[19−21] and models of chain packing[22] and membrane curvature.[23] When mixed after self-assembly (postmixed), the two species remained locally in the equilibrium states of the pure components, and a mixture of vesicles and spherical micelles was observed. The structures found when the two species were allowed partially to self-assemble before mixing (intermediate mixing) were more unusual and included paddle- and horseshoe-shaped aggregates. Using self-consistent field theory, we reproduced the transitions between morphologies observed in the premixed system and also details of the aggregates such as the bulbous ends of the rods.[19] We also gained insight into the complex structures seen at intermediate mixing by showing in SCFT calculations that the segregation of the two types of copolymer can stabilize regions of different curvature within a single aggregate.

In the current paper, we extend this study by varying the architectures of the copolymer species. We consider three specific cases: varying the length of the lamella-former in a blend of sphere- and lamella-formers, blending two lamella-formers of different lengths, and blending sphere-former with a polymer that has such a large hydrophobic block that it precipitates in solution if not mixed with more hydrophilic molecules. In all cases, we observe the quantitative and qualitative changes in the self-assembly as the copolymer architectures are changed. As in our previous work,[19] we perform self-consistent field theory calculations in tandem with our experiments and discuss how the distribution of the two copolymer species within the self-assembled structures leads to the formation of the structures seen in the experiments.

The article is organized as follows. In the following section, we give details of our experimental and theoretical methods. The Results section is divided into three subsections, one for each of the mixtures introduced above. We then present our conclusions.

METHODS

Materials. The PEO−PCL block copolymers were purchased from Advanced Polymer Materials Inc., Montreal, and used as received. GPC analysis was also provided by Advanced Polymer Materials Inc. and was referenced against PEO standards. Degrees of polymerization for the PCL block were calculated by ^{1}H NMR in $CDCl_3$ by comparison to the PEO block (the degrees of polymerization for the monomethoxypoly(ethylene oxides) used in these polymerizations are known). The volume fractions f_{EO} of the hydrophilic blocks were calculated from the melt densities of both blocks. We note that the simple volume fraction f_{EO} is not necessarily sufficient for very detailed studies of self-assembly and may need to be adjusted according to the chemical nature of the blocks.[24] Calculations based on the interfacial area per chain[14] can also provide a more accurate prediction of the morphologies of the self-assembled structures than the use of f_{EO}. However, in the current paper, we focus more on qualitative trends, and such steps are not necessary. The molecular weight and molecular weight distributions are given in Table 1. All other reagents with the exception of NMR solvents were purchased from Sigma-Aldrich Co. Ltd., Gillingham. Standard solvents were of spectrophotometric grade and inhibitor-free. Deuterated NMR solvents were purchased from Euriso-top S.A., Saint-Aubin. All solvents were filtered before use through Pall Acrodisc PSF GHP 200 nm filters. For all experiments, distilled and deionized Millipore water (resistivity = 18.2 MΩ·cm) was additionally filtered through Sartorius Ministart 200 nm filters directly before use.

Preparation of Solutions. Aqueous dispersions of block copolymer aggregates were prepared by dissolving the polymer in THF to a concentration of 10 mg mL^{-1}. These solutions were then mixed in the volume ratio noted for the experiments. All the mixing ratios are thus ratios of the masses of the respective polymers as opposed to molar ratios. Because of the close molecular weights (Table 1) of the two copolymers $PCL_{5K}PEO_{1K}$ and $PCL_{5K}PEO_{2K}$, these ratios are not very different in this case, while for the other combinations the conversion is easily calculated. Millipore water was added either manually or by an Eppendorf EDOS 5222 electronic dispensing system. 125 aliquots of 20 μL of water were added at 1 min intervals.

Turbidity Measurements. We performed turbidity measurements during the preparation of the samples using an adapted Perkin-Elmer UV/vis Lambda 40 spectrometer. A wavelength of 600 nm was used with a slit width of 2 nm. Stirring was performed using a standard magnetic stirrer/hot plate placed under the spectrometer. The polymer was dissolved in THF (1 mL, 10 mg mL^{-1}) and a zero reading was taken (transmittance, T = 100%). Millipore water was then added either in 10 μL aliquots every 30s using an Eppendorf EDOS 5222 electronic dispensing system, and a turbidity reading was taken after each addition.

Cryo-TEM. Samples for thin-film cryo-TEM were loaded onto plasma-treated (30 s) holey-carbon grids and prepared using a GATAN cryo-plunge into liquid ethane and then transferred using a GATAN 626 cryo-transfer system. Samples were examined using a JEOL 2100 TEM operating at 200 kV. Images were obtained using a Bioscan or a GATAN Ultrascan 4k camera and analyzed by GATAN Digital Micrograph version 1.71.38. During our previous investigations[14] we observed that imaging of the self-assembled structures (especially vesicles) is greatly improved in samples containing ca. 30% THF compared to samples in pure aqueous solution. Similar structures were observed in both solvent conditions, which indicates that at THF fractions of 30% and below the

mobility of the block copolymers is too restricted to allow for further growth of the aggregates. However, we found that, over a time scale of a few months, more complex aggregates (such as vesicles with an open flap[19]) were transformed into simple vesicles or nested onionlike structures. In order to focus on the initial structures that are formed (prior to any slow rearrangement processes) and to obtain as high-quality imaging as possible, we prepared the solutions for cryo-TEM in aqueous solutions containing 28% THF and imaged these samples within a maximum time of 2 weeks.

Self-Consistent Field Theory. To further our understanding of the role of polymer architecture on self-assembly, we performed self-consistent field theory (SCFT) calculations[4] on a model system of two species of AB diblock copolymers (lamella- and sphere-forming, respectively) in solution. Since we wish to focus on qualitative trends, we model the water−THF mixture by a simple A homopolymer and so neglect more subtle issues such as the amounts of the two components of the solvent in the cores of the self-assembled structures. SCFT is a coarse-grained mean-field theory in which the individual polymer molecules are modeled by random walks and composition fluctuations are neglected. For sufficiently long polymers,[25] these approximations prove extremely effective, and the predictions of the theory are very accurate, especially for polymer melts.[6] SCFT also yields much useful information on the self-assembly of block copolymers in solution, providing semiquantitative predictions of micelle morphology for homopolymer solvent[26,27] and qualitative predictions for molecular solvent.[19] As the length of the polymers is increased and fluctuations become less important, the SCFT predictions of micelle size and shape can become comparably accurate to those of much more expensive computational methods such as Monte Carlo.[28] We use a simple implementation of the theory where the interactions of the polymers are included by imposing incompressibility and introducing a contact potential between the A and B monomers.[6] The fine details of the polymer molecules are not taken into account, so that monomers of all species are taken to have the same length a and volume $1/\rho_0$.

From a technical point of view, a self-consistent field theory calculation consists of solving a series of differential (diffusion) equations to calculate the density profiles of the various polymer species. An initial guess for the profiles is made, which has the approximate form of the structure, such as a rod or a ring, that we wish to study. The density profiles are then recalculated until a set of equations reflecting the physical properties of the system (such as its incompressibility)[6,29] is satisfied. The SCFT differential equations are solved using a finite-difference method[30] with a spatial step size of $0.04aN^{1/2}$, where N is the number of monomers in the sphere-forming species, and reflecting boundary conditions are imposed at the origin and edges of the box. Full technical details of our calculation can be found in a recent publication.[21]

In the current paper, we use SCFT calculations in two slightly different ways. First, we perform effectively one-dimensional calculations on spherical micelles and infinite cylinders and bilayers to calculate simple phase diagrams as a function of sphere-former volume fraction and reproduce the basic phenomenology observed in the experiments. These calculations proceed as follows.[26,27] To begin, we calculate the free energy density of a box containing a single spherical, cylindrical, or planar aggregate surrounded by solvent. The shape of this box is set by the symmetry of the aggregate; for example, a spherical micelle is formed at the center of a spherical box. The calculation is therefore effectively one-dimensional. The volume V of this simulation box is then varied, keeping the volume fraction of copolymer constant, until the box size with the minimum free energy density is found. Provided the system is dilute, so that each aggregate is surrounded by a large volume of solvent and the aggregates do not interact with each other, this provides a simple model of a larger system (of fixed volume and fixed copolymer volume fraction) containing many aggregates. The reason for this is that such a system minimizes its free energy by varying the number of aggregates and hence the volume ("box size") occupied by each. Although computationally inexpensive, this approach yields accurate information on micelle shape transitions, and its results agree well with experiment.[26]

We also carry out more detailed calculations on the rod and ring structures seen in the experiment. We have two aims here. First, we wish to show that these more complex structures can be reproduced in detail in our calculations. Second, we will study the distribution of the sphere-forming and lamella-forming copolymers within the aggregates. Since both rods and rings have cylindrical symmetry, we will perform our (effectively two-dimensional) calculations in a cylindrical box. We note that it is not possible to include information on the distribution of the sphere- and lamella-formers within the micelles in the initial guess for the SCFT calculations. Any segregation of the two species will therefore arise naturally from the theory and need not be artificially introduced.[21] We perform our calculations at fixed compositions of the two copolymer species, as the slow rearrangement of the aggregates[19] suggests that the average composition of an aggregate is a slow variable.

Although this model is relatively simple, we found in our previous work on the self-assembly of binary PEO−PCL mixtures[19] that it contains enough detail to yield information on the structures formed in such systems and on the distribution of the two polymer species within these aggregates. In this earlier paper, we focused on a mixture of lamella-forming $PCL_{5K}PEO_{1K}$ and sphere-forming $PCL_{5K}PEO_{2K}$. We modeled the lamella-former by a symmetric AB diblock with equal numbers of monomers N_A and N_B in its hydrophilic (A) and hydrophobic (B) sections. For simplicity, the homopolymer was taken to have the same length as the lamella-former. In line with the experiments, the sphere-former contained the same number of hydrophobic monomers as the lamella-former but a larger number of hydrophilic monomers, so that $N_A = 3N_B$. The χ parameter setting the strength of the interaction between the A and B species was set to $\chi = 30/N$, where N is the total number of monomers in the sphere-forming species. Our aim here was not to match the experimental polymer parameters exactly, but to reproduce the basic phenomenology of the system (sphere- and lamella-forming species, matched hydrophobic blocks) as simply as possible. We take a similar approach in the current paper. To study the effect of lamella-former length on the blend of sphere- and lamella-former and to observe the result of blending two different lamella-formers, we introduce the larger lamella-forming copolymer PCL_{10K}-PEO_{2K}. We model this new molecule by an SCFT polymer with $3N/4$ monomers, while keeping $N_A = N_B$. The number of monomers $3N/4$ is chosen since increasing the size of the symmetric copolymer too much will lead to its forming micelles rather than bilayers.[12,13] For the sake of clarity, we summarize the SCFT polymer parameters introduced above in Table 2.

Table 2. Parameters of the Polymers Used in SCFT Calculations[a]

polymer	sample code	SCFT monomers	SCFT N_A/N_B
lamella-former (long)	$PCL_{10K}PEO_{2K}$	$3N/4$	1
lamella-former (short)	$PCL_{5K}PEO_{1K}$	$N/2$	1
sphere-former	$PCL_{5K}PEO_{2K}$	N	3
solvent	n/a	$N/2$	n/a

[a] For each SCFT polymer, we list the corresponding polymer in the experiments, the number of (SCFT) monomers, and the volume ratio of the hydrophilic and hydrophobic blocks.

RESULTS

Blends of Lamella- and Sphere-Formers. To begin, we consider the structures formed when various concentrations of

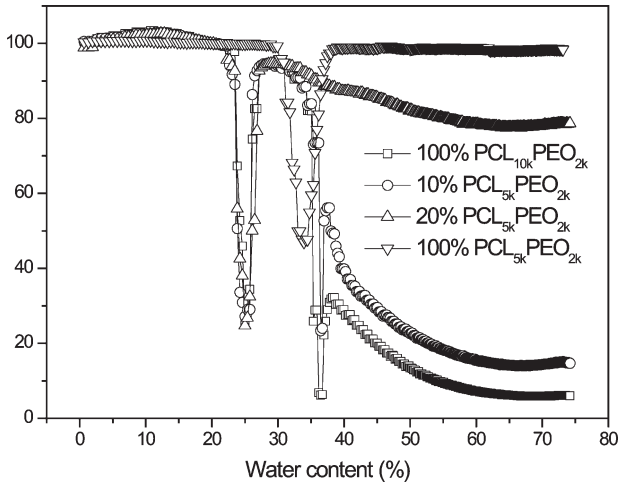

Figure 1. Turbidity traces for the self-assembly of block copolymer mixtures of $PCL_{10K}PEO_{2K}$ and $PCL_{5K}PEO_{2K}$. The optical transmission (in %) at 600 nm is plotted against the water concentration in the solvent.

the sphere-forming copolymer $PCL_{5K}PEO_{2K}$ are added to the long lamella-former $PCL_{10K}PEO_{2K}$. These molecules are chosen to isolate the effect of molecular weight on the shape transitions: they contain more monomers than the $PCL_{5K}PEO_{1K}$ copolymers studied previously but have the same ratio of hydrophobic to hydrophilic blocks. We first turn our attention to the turbidity traces of this system. The features in a turbidity trace can be directly linked to the points where the transitions between spherical micelles, wormlike micelles, and vesicles occur.[14] Specifically, in clear solutions spherical micelles or short worms dominate, and no or very few vesicles are present. Conversely, high turbidity of the solution at high water content indicates the presence of larger aggregates such as vesicles.[14] From these measurements (Figure 1) it can be seen that a mixture of 10% $PCL_{5K}PEO_{2K}$ with 90% $PCL_{10K}PEO_{2K}$ does not behave very differently from a system of pure lamella-former, since the traces for the two systems are very similar. However, a sharp change in the optical transmission is seen on addition of 20% PCL_{5K}-PEO_{2K}. Here, although the concentration of sphere-former is still relatively low, the trace resembles that of pure $PCL_{5K}PEO_{2K}$ much more closely than that of the pure lamella-former $PCL_{10K}PEO_{2K}$ and does not show the strong turbidity in the water-rich area linked with the presence of larger aggregates.[14] We note in passing that the sharp dip in the optical transmission between 20% and 30% water is most probably due to a miscibility gap in the PEO−THF−water phase space[14,31,32] and is not associated with a transition in the shape of the aggregates.

These results are in contrast to those obtained for mixtures of $PCL_{5K}PEO_{1K}$ and $PCL_{5K}PEO_{2K}$ in our previous publication.[19] There, vesicles were formed up to ∼30% sphere-former, whereas in the current system the transition from vesicles to micelles occurs between 10% and 20% $PCL_{5K}PEO_{2K}$. Increasing the length of the lamella-forming copolymer is therefore seen to favor the formation of more curved structures.

To gain more detailed insights into the system, we now consider cryo-TEM images taken at a range of sphere-former concentrations. In mixes with 90% $PCL_{10K}PEO_{2K}$ and 10% $PCL_{5K}PEO_{2K}$, this technique reveals the presence of a large variety of structures, as can be seen in Figure 2. First, we note that

Figure 2. Cryo-TEM of a mixture of 90% $PCL_{10K}PEO_{2K}$ and 10% $PCL_{5K}PEO_{2K}$ self-assembled by solvent exchange from THF. The images were taken in an aqueous solution with 28% THF; the scale bars are 500 nm.

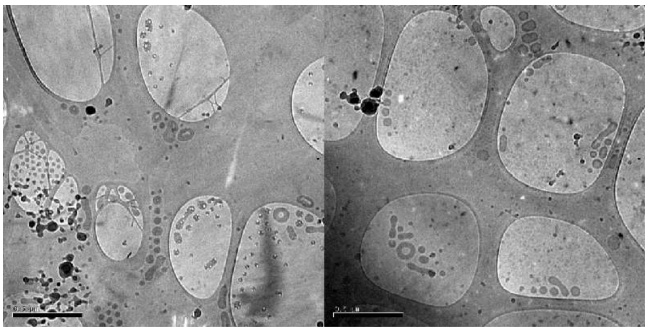

Figure 3. Cryo-TEM of a mixture of 80% $PCL_{10K}PEO_{2K}$ and 20% $PCL_{5K}PEO_{2K}$ self-assembled by solvent exchange from THF. The images were taken in an aqueous solution with 28% THF; the scale bars are 500 nm.

a significant number of vesicles is still present, accounting for the high turbidity of this mixture seen in Figure 1. In addition, wormlike micelles and rings (end-to-end joined worms) can be seen in the left image. The wormlike micelles here often form branched network structures showing multiple three-way connections. The individual branches of the network also tend to be rather short, terminating in enlarged end-caps. These images closely resemble some of those shown by Jain and Bates[2] for PEO-*b*-PB block copolymer mixtures as well as those of Chen et al.[33] for PS-*b*-PAA. In different regions of the same TEM grid, very unusual vesicles could also be seen that on drying deformed to create a space-filling tessellated pattern (Figure 2, right image). The majority of these structures clearly show the dark outer ring of the vesicle wall confirming that they are indeed closed vesicles. However, on the top right there are some structures that do not have this pronounced darker rim and may therefore be unwrapped bilayer sheets. Such structures have been proposed as intermediate stages in the self-assembly of vesicles.[34,35]

At a mixing ratio of 80% $PCL_{10K}PEO_{2K}$ and 20% PCL_{5K}-PEO_{2K} (Figure 3), the TEM shows a mix of spherical micelles, short worms, and toroidal rings. The vesicles and sheetlike structures shown in Figure 2 no longer appear at this concentration. This is in line with the turbidity trace results: this solution is clear at high water concentrations, consistent with the presence of small micelles such as rings and short rods.[14]

We now present our self-consistent field theory calculations on our simple model of our experimental systems. For each set of calculations, we first consider the $PCL_{5K}PEO_{1K}$−$PCL_{5K}PEO_{2K}$

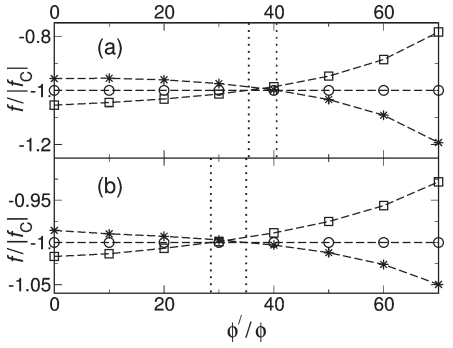

Figure 4. Free energy densities as a function of mixing ratio for (a) a short symmetric lamella-former with $N/2$ monomers blended with a N-monomer sphere-former and (b) a longer symmetric lamella-former with $3N/4$ monomers blended with a N-monomer sphere-former. The free energy densities for spherical micelles, cylindrical micelles, and flat bilayers are plotted with stars, circles, and squares, respectively. The transitions between the different micelle morphologies are indicated by vertical dashed lines.

mixture studied in our previous paper,[19] modeled, as described in the Methods section, by a polymer blend including relatively short symmetric lamella-formers containing $N/2$ monomers and sphere-formers containing N monomers. Next, we move on to our model of the $PCL_{10K}PEO_{2K}$−$PCL_{5K}PEO_{2K}$ system of the current paper, in which the SCFT lamella-formers are still symmetric but now contain $3N/4$ monomers, and look at how the self-assembly is altered by the change in polymer architecture.

To begin, we calculate the free energy densities of ideal spheres, infinite cylinders, and infinite bilayers using the method of variable subsystem size described above and determine how these vary as the volume fraction of sphere-former is increased. To ensure that the system is relatively dilute and that aggregates are surrounded by a large volume of solvent, we fix the overall volume fraction of copolymer to 8%. All free energy densities F/V are plotted with respect to that of the homogeneous solution with the same composition F_h/V; that is, we plot the quantity $f = F/V - F_h/V$. Since the free energy densities f_i of the three shapes of aggregate are quite close together, they are plotted normalized with respect to the magnitude of the free energy density $|f_C|$ of the cylindrical micelle to show the shape transitions clearly. The cylinder free energy density then appears as a horizontal line at $f = -1$ and is approached from above and below by the sphere and lamella free energy densities as the sphere-former concentration increases.

Figure 4 shows the free energy densities of spherical, cylindrical, and planar aggregates plotted against φ'/φ, where φ' is the volume fraction of sphere-former and φ is the total volume fraction of copolymer (sphere-formers plus lamella-formers). Panel a shows the results for the system with the shorter lamella-former of $N/2$ monomers.[19] In this system, the lamella-former has the lowest free energy at lower sphere-former volume fractions. At around $\varphi'/\varphi = 35\%$, the lamellar and cylindrical free energies cross, and the cylinder has the lowest free energy until $\varphi'/\varphi \approx 40\%$, when the spherical micelle finally becomes most energetically favorable. This reproduces the series of transitions from vesicles to cylindrical micelles (worms and rings) to spherical micelles seen in our experiments,[19] although the values of φ'/φ at which the transitions occur are slightly shifted, as would be expected in view of the simplicity of our model. In these TEM images,[19] vesicles were seen at 5% and 25% sphere-forming copolymer and spherical micelles are seen at 75% sphere-former, in line with our calculations. However, a mixture of worms, rings, and vesicles is seen at 50%, where our calculations predict spherical micelles. It is interesting to note that both our calculations and experiments demonstrate that a blend of sphere-forming and lamella-forming amphiphiles can form cylindrical micelles, even though this structure is favored by neither of these molecules individually.[21]

In panel b of Figure 4, we plot the corresponding free energy densities for the same system but with the degree of polymerization of the symmetric lamella former increased to $3N/4$ monomers: a simple representation of the longer $PCL_{10K}PEO_{2K}$ molecules of the current system. Again, we find the same sequence of morphologies as the sphere-former concentration is increased. However, as in the experiments, the vesicle−cylinder and cylinder−sphere transitions are shifted to lower sphere-former volume fractions with respect to the previous system.[19] Specifically, the former transition now occurs at approximately $\varphi'/\varphi = 28\%$, while the latter is moved to around $\varphi'/\varphi = 35\%$. Again, due to the simplicity of our theoretical approach, these transitions are not perfectly aligned with those in the experimental system. For example, the TEM images taken at a mixing ratio of 20% (Figure 3) show a mixture of rings, short rods, and spherical micelles, whereas our theory predicts that this mixture will form vesicles, or, equivalently, that the region of coexistence of morphologies would be expected at a mixing ratio closer to 30%.

A restriction of our SCFT approach is that it does not explicitly deal with the coexistence of different morphologies, such as spheres and cylinders, that is often seen in the TEM images. This is related to the fact that we consider aggregates of fixed composition in our calculations. In reality, demixing of the two components may occur, so that, for example, a spherical micelle will contain a larger fraction of sphere-forming copolymers than a wormlike micelle.

We believe that the shift in the shape transitions to lower sphere-former volume fractions for increasing chain length of the lamella-former is primarily due to the greater shape asymmetry of the lamella-former when its length is increased while keeping the ratio of the hydrophilic and hydrophobic blocks constant. This can be seen from the following heuristic scaling model of the shape asymmetry of diblock copolymers. Although our system is not strictly in the scaling regime (since the two blocks of the copolymer are only weakly immiscible), this approach still yields insight into the basic trends in micelle shape as molecular weight is varied. We assume that the hydrophilic block A of the lamella-former is swollen by solvent and so has an end-to-end distance[36] of $R_A \sim N_A^{3/5}$ and effective volume $V_A \sim R_A^3 \sim N_A^{9/5}$. In contrast, the hydrophobic B-blocks are taken to be in a collapsed, brushlike state,[37] and so have effective volume $V_B \sim N_B$. Since we keep the ratio of the hydrophilic and hydrophobic blocks constant, we can also write $V_A \sim N_{tot}^{9/5}$ and $V_B \sim N_{tot}$, where $N_{tot} = N_A + N_B$ is the total length of the lamella-former. Defining the shape asymmetry of the lamella-former to be $\varepsilon = V_A/V_B$, we have $\varepsilon \sim N_{tot}^{4/5}$. Therefore, as we increase N_{tot} at constant hydrophilic to hydrophobic ratio, ε will also increase and the lamella-former will become more asymmetric. In consequence, we expect it to have an greater tendency to form curved structures, with the swollen A-blocks on the outside of the curved surface. This shift toward more curved aggregates as the overall copolymer length is increased has indeed been seen in experiments on symmetric diblock copolymers in solution.[13]

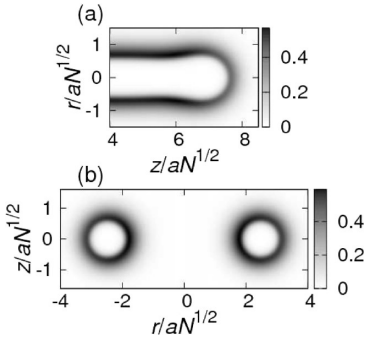

Figure 5. Bulbous-ended rod (a) and ring (b) structures in a system with a long symmetric lamella-former with $3N/4$ monomers blended with a N-monomer sphere-former in a ratio of 2 to 1. The total density of the hydrophilic A-blocks is plotted in cylindrical polar coordinates.

In the above calculations, we have studied only infinite cylinders. However, the cylindrical micelles seen in the experiments have the form of rings or short, bulbous-ended rods. We now use effectively 2d SCFT calculations in cylindrical polar coordinates[19,21] to study these structures in more detail. First, in Figure 5, we demonstrate that these structures can indeed be reproduced within our model's parameter space. We focus on a system of lamella-former with $3N/4$ monomers mixed with sphere-former in a ratio of 2 to 1: a blending ratio where cylindrical micelles have the lowest free energy in our calculations (Figure 4). To show the form of the structures, the sum of the hydrophilic block densities of the two species is plotted. Panel a of Figure 5 shows the bulbous end of a rod,[38] preceded by a thinner neck region of negative curvature.[39,40] We find also that ringlike structures exist as local solutions to SCFT and plot a cross section through one of these aggregates in panel b.

We now turn our attention to the distribution of the two copolymer species within the cores of the rod structures. To this end, we introduce an enhancement factor[19,21] $\eta(\mathbf{r})$, which we define as

$$\eta(\mathbf{r}) = \frac{\varphi_{B2}(\mathbf{r})}{\varphi_{B}(\mathbf{r})}\frac{\overline{\varphi}_{B}}{\overline{\varphi}_{B2}} \qquad (1)$$

Here, $\varphi_B(\mathbf{r})$ is the local volume fraction of lamella-former hydrophobic blocks and $\varphi_{B2}(\mathbf{r})$ is the corresponding quantity for the sphere-former hydrophobic blocks. The mean volume fractions of the two species are denoted by $\overline{\varphi}_B$ and $\overline{\varphi}_{B2}$. The enhancement factor tells us how much the concentration of sphere-former is enhanced with respect to that of the lamella-former at a given point in the system. We define $\eta(\mathbf{r})$ such that it is normalized with respect to the mean volume fractions of the two core species, so that values greater than one represent enhancement of the sphere-former concentration and values less than one represent depletion. The enhancement factor is plotted only within the core of the micelle, defined as the region where the total density of the hydrophobic species $\varphi_B(\mathbf{r}) + \varphi_{B2}(\mathbf{r})$ is greater than that of the hydrophilic species $\varphi_A(\mathbf{r}) + \varphi_{A2}(\mathbf{r})$.

To locate this region accurately, we apply simple bilinear interpolation to our SCFT data to make the grid finer before plotting $\eta(\mathbf{r})$. In Figure 6a, we show the enhancement factor for the blend of sphere-former and shorter lamella-former ($N/2$ monomers).[19] In this system, the sphere-formers segregate to the end of the rod,[19] which is the most strongly curved part of the aggregate and, in fact, closely resembles a spherical micelle. Since

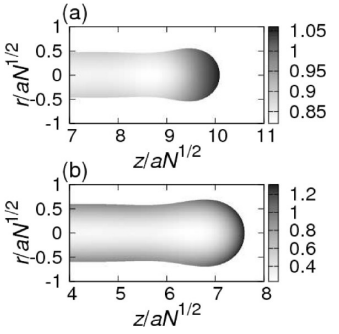

Figure 6. Enhancement factor $\eta(\mathbf{r})$ plotted within the cores of micelles formed from (a) a 2:1 blend of $N/2$-monomer lamella-former and N-monomer sphere-former and (b) a 2:1 blend of $3N/4$-monomer lamella-former and N-monomer sphere-former. Dark areas show regions where the concentration of the sphere-former is enhanced with respect to the lamella-former, and lighter areas show regions where it is depleted.

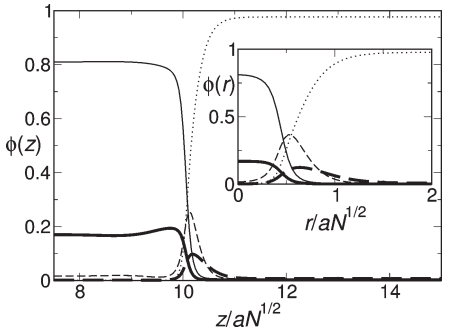

Figure 7. Cuts through the density profiles of the rod structure in a 2:1 blend of $N/2$-monomer lamella-former and N-monomer sphere-former. The hydrophobic and hydrophilic block density profiles are shown with full and dashed lines, respectively, and the sphere-formers are plotted with thicker lines. The solvent is plotted with a dotted line. The main panel shows a cut along the main axis of the rod, and the inset shows a cut perpendicular to this axis at the center of the rod.

the hydrophobic blocks of the two species are matched and so can both reach the center of the micelle, the ratio of the concentrations of the two species varies rather little in the main cylindrical body of the aggregate away from the end-caps. This is in contrast to the system shown in panel b of Figure 6, where a longer lamella-former of $3N/4$ monomers is used. Here, the sphere-formers have shorter hydrophobic blocks than the lamella-formers and no longer reach the central axis of the cylindrical micelle. This means that the sphere-former concentration is enhanced on the surface of the body of the cylinder as well as in the end-cap and is strongly depleted in the center of the rod. We note also that this mismatch between the hydrophobic blocks means that segregation is a stronger effect than in the previous system, with the range of values taken by $\eta(\mathbf{r})$ significantly increased.

A similar segregation of amphiphiles according to curvature has also recently been seen in more microscopic dissipative particle dynamics simulations,[41] where an eventual splitting-off of the end-cap to form a spherical micelle is seen. Although we do not explicitly consider this effect here, SCFT is capable of modeling the similar phenomenon of the destabilization of junctions connecting threadlike micelles to flat bilayers as sphere-forming amphiphile is added.[21]

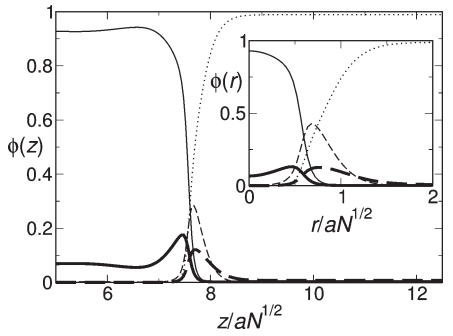

Figure 8. Cuts through the density profiles of the rod structure in a 2:1 blend of $3N/4$-monomer lamella-former and N-monomer sphere-former. The hydrophobic and hydrophilic block density profiles are shown with full and dashed lines, respectively, and the sphere-formers are plotted with thicker lines. The solvent is plotted with a dotted line. The main panel shows a cut along the main axis of the rod, and the inset shows a cut perpendicular to this axis at the center of the rod.

To study the distribution of the sphere- and lamella-formers within the micelles in more detail, we now plot cuts through the density profiles of the various species both along and perpendicular to the axis of the cylinder for the two systems shown in Figure 6. The plot for the system with shorter lamella-formers (Figure 7) confirms two points made above. First, it can be seen from the cut along the rod axis shown in the main panel of Figure 7 that the segregation of the sphere-formers to the end-cap is relatively weak and that the peak in sphere-former concentration here is quite small. Furthermore, from the inset to Figure 7, which shows a cut perpendicular to the rod axis at the center of the micelle, we see that there is no segregation of the two polymer species in the main body of the aggregate. In corresponding plots for the system with longer lamella-formers (Figure 8), we see strong segregation of the sphere-formers to both the end-caps and surface of the cylinder. In addition, plotting the data in this way also shows us that, despite the new effect of the enhancement of sphere-former concentration on the surface of the cylinder, the strongest segregation is still to the most highly curved region: the end-caps. To see this, note that the peak in sphere-former concentration at the end of the rod (main panel of Figure 8) is higher and more pronounced than that at the surface of the cylindrical section of the rod (inset to Figure 8). We note also that the sphere-formers have a dip in concentration just before the peak at the cylinder end-cap. This feature corresponds to the negatively curved neck of the micelle[40] visible in Figure 6. Since the sphere-formers naturally prefer positive curvature, they migrate away from this region.

We believe that the stronger segregation of the sphere-formers in the mixture with the longer lamella-former is due to the entropic elasticity of the core blocks. Specifically, if the sphere-formers were homogeneously mixed with the longer lamella-formers, the hydrophobic cores would have to be strongly stretched, restricting the number of configurations they can access and so leading to a loss of entropy. In consequence, the sphere-formers move to the end-caps, leading to the formation of short cylinders or network structures with many bulbous end-caps such as those seen in Figure 2.

The larger number of Y-junctions[42] in the $PCL_{10K}PEO_{2K}$ system compared to the previous $PCL_{5K}PEO_{1K}$ system[19] may be explained in a similar way:[1] in the system containing the shorter lamella-former $PCL_{5K}PEO_{1K}$, the relatively short core blocks can adopt a smaller number of conformations and so are less able to pack into a more complex structure such as a Y-junction. The increased number of branched structures at higher molecular weights is in agreement with the work of several other groups[1,33,43,44] on single-component systems.

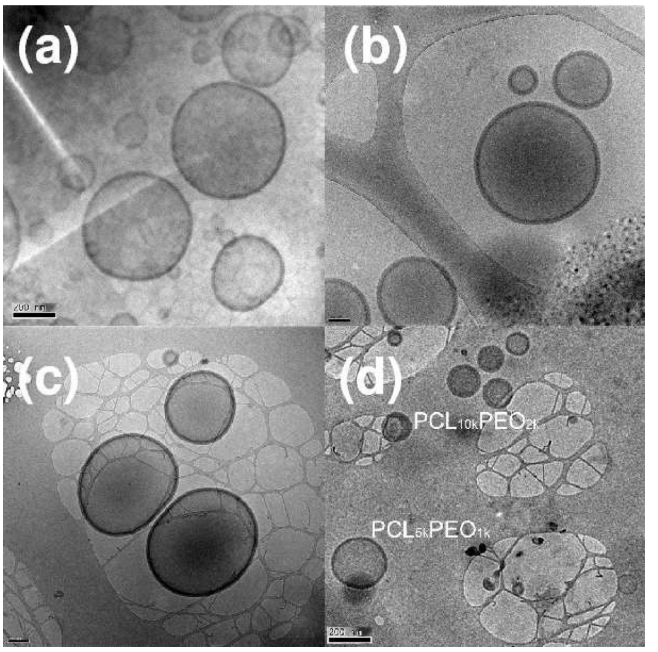

Figure 9. Cryo-TEM images of the vesicles in 28% THF in water. Panels a and b show the vesicles obtained from the self-assembly of $PCL_{5K}PEO_{1K}$ and $PCL_{10K}PEO_{2K}$, respectively. Panel c shows the structures obtained when solutions of $PCL_{5K}PEO_{1K}$ and $PCL_{10K}PEO_{2K}$ in pure THF are mixed in equal parts prior to self-assembly. Panel d shows the same composition when the two solutions are mixed after self-assembly at a THF content of 28%. The image was taken 1 week after mixing. Two distinct populations of vesicles with different wall thickness can be seen. All images are at the same magnification. The scale bars in (a) and (d) are 200 and 100 nm in panels b and c.

Blends of Two Lamella-Formers. Having studied the effect of blending two copolymers that individually form different structures, we now investigate a system where the two species are lamella-formers but of different lengths. The two copolymers considered are the shorter $PCL_{5K}PEO_{1K}$[19] and the longer $PCL_{10K}PEO_{2K}$ molecule introduced above. As in our previous publication,[19] we mixed the two polymers both before and after their individual self-assembly.

Figure 9 shows representative cryo-TEM images of the vesicles formed by $PCL_{5K}PEO_{1K}$ (panel a) and $PCL_{10K}PEO_{2K}$ (panel b) on their own. In the second row of the figure the vesicles are shown that result when the two block copolymers are mixed before assembly (in pure THF solution) (panel c) and after assembly, i.e., after dilution to 28% THF (panel d). This latter case corresponds to mixing the solutions shown in panels a and b of Figure 9. As the chain lengths of the two copolymers differ by a factor of 2, the resulting vesicles have different wall thickness (16 and 25 nm, respectively). In image d of the sample mixed postassembly, the wall thicknesses of the individual vesicles remain unchanged and two different populations can be clearly distinguished, while in the sample mixed preassembly an intermediate wall thickness of ca. 20 nm is found. This result indicates that, as before,[19] the exchange of material between the different structures is suppressed at THF concentrations below 28%.

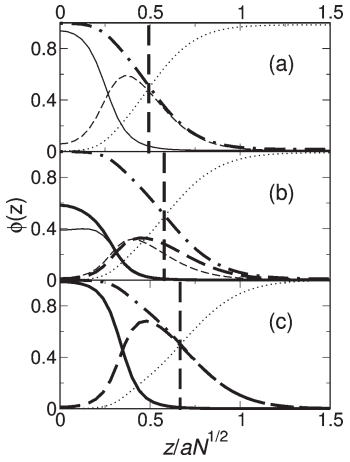

Figure 10. Density profiles of an infinite lamellar structure in (a) an $N/2$-monomer lamella-former, (b) a 1:1 blend of $3N/4$-monomer lamella-former and $N/2$-monomer lamella-former, and (c) a $3N/4$-monomer lamella-former. The hydrophobic and hydrophilic block density profiles are shown with full and dashed lines, respectively, and the $3N/4$ lamella-formers are plotted with thicker lines. The solvent is plotted with a dotted line, the total density of copolymers is plotted with a dot-dashed line, and the point at which these two densities are equal is marked with a thick vertical dashed line.

We now wish to see whether the result of the blending of two types of lamella-former leading to the formation of vesicles of intermediate wall thickness can be reproduced in our simple SCFT model. In panel a of Figure 10, we plot the density profiles of the hydrophobic B-blocks, hydrophilic A blocks, and solvent of a bilayer formed of relatively short lamella-formers of $N/2$ monomers calculated, as above, from the method of variable subsystem size. We also show the total density profile of the copolymers (A blocks plus B blocks) and the bilayer thickness, defined as the distance from the origin at which the densities of copolymer and solvent are equal. Panel c shows the corresponding profiles for the longer lamella former with $3N/4$ monomers. As expected from the respective lengths of the molecules, this latter polymer forms thicker bilayers than those shown in panel a. In the central panel b, we show the density profiles for a bilayer formed of an equal-parts mixture of the two species. In excellent agreement with the experiments, this mixed bilayer has a thickness approximately halfway between those of the pure bilayers. By comparing the density profiles in panels a and b, we see that the addition of the longer species (in panel b) causes the core blocks of the shorter species to stretch outward from their equilibrium state in a single-component structure (panel a).

Strongly Hydrophobic Copolymer Mixed with Micelle Former. Finally, we investigate an extreme case of two strongly mismatched copolymers. The first of these, $PCL_{5K}PEO_{550}$, is so hydrophobic that, in isolation, it fails to assemble into vesicles and precipitates instead. This polymer was mixed with the micelle-former considered above, $PCL_{5K}PEO_{2K}$. The two species were mixed before their individual self-assembly in a mass ratio of 60% $PCL_{5K}PEO_{550}$ to 40% $PCL_{5K}PEO_{2K}$. When self-assembly was triggered by the addition of water, the solution became turbid, indicating the presence of large aggregates. This was confirmed by cryo-TEM (Figure 11), which revealed the presence of a large fraction of vesicles with smaller populations of wormlike and spherical micelles. Remarkably, many of these vesicles are not spherical but have a novel elongated shape, which

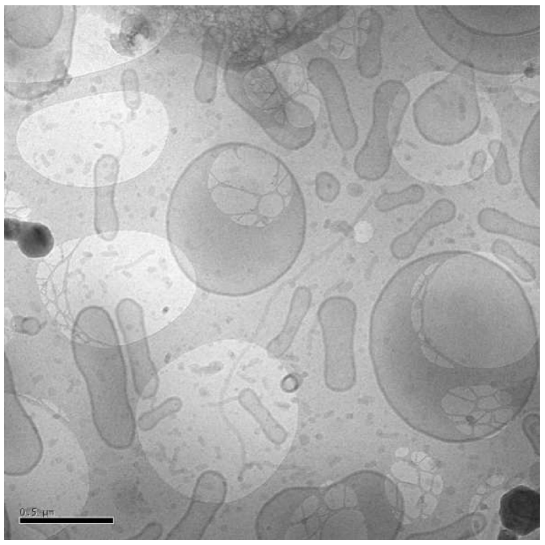

Figure 11. Cryo-TEM of the self-assembled structures obtained for a mixture of $PCL_{5K}PEO_{550}$ and $PCL_{5K}PEO_{2K}$ at a mass-based mixing ratio of 3 to 2 parts. The image was taken from a solution containing 28% THF, and the scale bar is 500 nm.

could be due to segregation of the two copolymer species within the individual aggregates. This is likely to be an especially strong effect in the current system, as the solubilities of the two copolymer species are very different and the $PCL_{5K}PEO_{550}$ chains start to aggregate at much lower water fractions than the more hydrophilic $PCL_{5K}PEO_{2K}$. This produces a phenomenon analogous to the intermediate mixing discussed in our earlier work:[19] the strongly hydrophobic chains are partially self-assembled at the time they encounter the sphere-formers. In consequence, the two species mix less efficiently, and regions of different curvature can coexist within the same aggregate.[19] The negative curvature regions around the centers of the elongated vesicles are likely to contain higher concentrations of the strongly hydrophobic copolymer, whereas the curved ends of these structures will probably contain more of the micelle-former. Because of the small difference in curvature between the different regions of the aggregate, testing this hypothesis is unfortunately beyond the scope of our current SCFT methods.

■ CONCLUSION

In this paper, we have used a combination of experiment and theory to show that varying the chain geometry of binary copolymer mixtures in solution can give us precise control over the form of the self-assembled aggregates and lead to the formation of new structures. We investigated three distinct situations. First, we studied a mixture of sphere-forming and lamella-forming copolymers and found in both electron microscopy experiments and coarse-grained mean-field theory that increasing the chain length of the lamella-former while keeping the ratio of its hydrophilic and hydrophobic components constant leads to the formation of highly curved structures at lower sphere-former volume fractions. We presented an explanation of this behavior in terms of the volume asymmetry of the two sections of the diblock. Using more detailed SCFT calculations, we found the rings and bulbous-ended rods seen in the experiments and observed a strong segregation of the sphere-forming copolymers to the curved ends of the cylindrical micelles. We

explained this effect by suggesting that sphere-forming copolymers would pay a large free energy penalty if they were dispersed evenly through the aggregates, as their relatively short core blocks would need to be strongly stretched to fit in with those of the lamella-former. In consequence, the sphere-formers tend to demix from the lamella-formers, leading to the formation of cylinders with highly curved end-caps. This segregation between species may be accentuated by other effects such as enthalpy of crystallization. We also studied a mixture of two lamella-forming copolymers of different molecular weights. In both experiment and theory, we found that the bilayers formed in this system have a wall thickness that is in between those observed in systems containing only one of the two types of lamella-former. Finally, a mixture of sphere-forming copolymer and a strongly hydrophobic copolymer that precipitates in isolation was shown to form a range of structures, including novel elongated vesicles.

The results presented above demonstrate the power of a combined experimental and theoretical approach to the investigation and design of self-assembling block copolymers. Self-consistent field theory can map out the broad phase diagram of block copolymer mixtures and suggest experimental parameter spaces to search for new morphologies. Furthermore, it yields insights into the aggregates observed in the experiments, reproducing details of the structures and the distribution of the different polymer species within these. The wealth of morphologies observed in our work highlights the fine balance of forces governing the self-assembly behavior of block copolymer systems. Further investigation of the different factors could open up a new zoo of self-assembled aggregates with the distribution and magnitude of local curvature differences as additional design parameters, and several avenues for extension of this work suggest themselves. In particular, the precise role of the sphere-former architecture could be investigated, with the aim of producing structures of a specified curvature. The various components could also be mixed at different stages in their self-assembly,[19] to access further new aggregates and to gain insight into the intermediate steps in micelle and vesicle formation. On the theoretical side, our SCFT calculations could be extended to investigate the favorability of the more complex structures, particularly the Y-junctions, in different copolymer mixtures.

AUTHOR INFORMATION

Corresponding Author

*E-mail: peter.schuetz@unilever.com.

ACKNOWLEDGMENT

This work was performed in Project 264 of the Micro and Nanotechnology Scheme part-funded by the UK Technology Strategy Board (formerly DTI). Unilever is thanked for permission to publish this work. M.J.G. is currently funded by the EU under a FP7 Marie Curie fellowship.

REFERENCES

(1) Jain, S.; Bates, F. S. *Science* **2003**, *300*, 460–464.
(2) Jain, S.; Bates, F. S. *Macromolecules* **2004**, *37*, 1511–1523.
(3) Smart, T. P.; Lomas, H.; Massignani, M.; Flores-Merino, M. V.; Perez, L. R.; Battaglia, G. *Nano Today* **2008**, *3*, 38–46.
(4) Edwards, S. F. *Proc. Phys. Soc.* **1965**, *85*, 613–624.
(5) Schmid, F. *J. Phys.: Condens. Matter* **1998**, *10*, 8105–8138.
(6) Matsen, M. W. In *Soft Matter*; Wiley-VCH: Weinheim, 2006; Chapter 2.
(7) Maniadis, P.; Lookman, T.; Kober, E. M.; Rasmussen, K. O. *Phys. Rev. Lett.* **2007**, *99*, 048302.
(8) Drolet, F.; Fredrickson, G. H. *Phys. Rev. Lett.* **1999**, *83*, 4317–4320.
(9) Kim, Y.; Dalhaimer, P.; Christian, D. A.; Discher, D. E. *Nanotechnology* **2005**, *16*, S484–S491.
(10) Discher, B. M.; Won, Y. Y.; Ege, D. S.; Lee, J. C. M.; Bates, F. S.; Discher, D. E.; Hammer, D. A. *Science* **1999**, *284*, 1143–1146.
(11) Discher, D. E.; Eisenberg, A. *Science* **2002**, *297*, 967–973.
(12) Kinning, D. J.; Winey, K. I.; Thomas, E. L. *Macromolecules* **1988**, *21*, 3502–3506.
(13) Kaya, H.; Willner, L.; Allgaier, J.; Richter, D. *Appl. Phys. A: Mater. Sci. Process.* **2002**, *74*, S499–S501.
(14) Adams, D. J.; Kitchen, C.; Adams, S.; Furzeland, S.; Atkins, D.; Schuetz, P.; Fernyhough, C. M.; Tzokova, N.; Ryan, A. J.; Butler, M. F. *Soft Matter* **2009**, *5*, 3086–3096.
(15) Sorre, B.; Callan-Jones, A.; Manneville, J. B.; Nassoy, P.; Joanny, J. F.; Prost, J.; Goud, B.; Bassereau, P. *Proc. Natl. Acad. Sci. U. S.A.* **2009**, *106*, 5622–5626.
(16) Zidovska, A.; Ewert, K. K.; Quispe, J.; Carragher, B.; Potter, C. S.; Safinya, C. R. *Langmuir* **2009**, *25*, 2979–2985.
(17) Vinson, P. K.; Talmon, Y.; Walter, A. *Biophys. J.* **1989**, *56*, 669–681.
(18) Oberdisse, J.; Regev, O.; Porte, G. *J. Phys. Chem. B* **1998**, *102*, 1102–1108.
(19) Schuetz, P.; Greenall, M. J.; Bent, J.; Furzeland, S.; Atkins, D.; Butler, M. F.; McLeish, T. C. B.; Buzza, D. M. A. *Soft Matter* **2011**, *7*, 749–759.
(20) Li, F.; Marcelis, A. T. M.; Sudholter, E. J. R.; Stuart, M. A. C.; Leermakers, F. A. M. *Soft Matter* **2009**, *5*, 4173–4184.
(21) Greenall, M. J.; Gompper, G. *Langmuir* **2011**, *27*, 3416–3423.
(22) Fattal, D. R.; Andelman, D.; Ben-Shaul, A. *Langmuir* **1995**, *11*, 1154–1161.
(23) Andelman, D.; Kozlov, M. M.; Helfrich, W. *Europhys. Lett.* **1994**, *25*, 231–236.
(24) Rajagopal, K.; Mahmud, A.; Christian, D. A.; Pajerowski, J. D.; Brown, A. E. X.; Loverde, S. M.; Discher, D. E. *Macromolecules* **2010**, *43*, 9736–9746.
(25) Müller, M. In *Soft Matter*; Wiley-VCH: Weinheim, 2006; Chapter 3.
(26) Greenall, M. J.; Buzza, D. M. A.; McLeish, T. C. B. *J. Chem. Phys.* **2009**, *131*, 034904.
(27) Greenall, M. J.; Buzza, D. M. A.; McLeish, T. C. B. *Macromolecules* **2009**, *42*, 5873–5880.
(28) Cavallo, A.; Müller, M.; Binder, K. *Macromolecules* **2006**, *39*, 9539–9550.
(29) Matsen, M. W. *J. Chem. Phys.* **2004**, *121*, 1938–1948.
(30) Press, W. H.; Flannery, B. P.; Teukolsky, S. A.; Vetterling, W. T. *Numerical Recipes in C*, 2nd ed.; Cambridge University Press: Cambridge, 1992.
(31) Cristobal, G.; Berret, J. F.; Chevallier, C.; Talingting-Pabalan, R.; Joanicot, M.; Grillo, I. *Macromolecules* **2008**, *41*, 1872–1880.
(32) Schuhmacher, E.; Soldi, V.; Pires, A. T. N. *J. Membr. Sci.* **2001**, *184*, 187–196.
(33) Chen, L.; Shen, H. W.; Eisenberg, A. *J. Phys. Chem. B* **1999**, *103*, 9488–9497.
(34) Lasic, D. D. *Biochem. J.* **1988**, *256*, 1–11.
(35) Antonietti, M.; Forster, S. *Adv. Mater.* **2003**, *15*, 1323–1333.
(36) Jones, R. A. L. *Soft Condensed Matter*; Oxford University Press: Oxford, 2002.
(37) Safran, S. A. *Statistical Thermodynamics of Surfaces, Interfaces, and Membranes*; Westview Press: Boulder, 1994.
(38) Bernheim-Groswasser, A.; Zana, R.; Talmon, Y. *J. Phys. Chem. B* **2000**, *104*, 4005–4009.
(39) Jódar-Reyes, A. B.; Leermakers, F. A. M. *J. Phys. Chem. B* **2006**, *110*, 6300–6311.

(40) Jódar-Reyes, A. B.; Leermakers, F. A. M. *J. Phys. Chem. B* **2006**, *110*, 18415–18423.
(41) Loverde, S. M.; Ortiz, V.; Kamien, R. D.; Klein, M. L.; Discher, D. E. *Soft Matter* **2010**, *6*, 1419–1425.
(42) Dan, N.; Safran, S. A. *Adv. Colloid Interface Sci.* **2006**, *123*, 323–331.
(43) Won, Y. Y.; Brannan, A. K.; Davis, H. T.; Bates, F. S. *J. Phys. Chem. B* **2002**, *106*, 3354–3364.
(44) Dan, N.; Shimoni, K.; Pata, V.; Danino, D. *Langmuir* **2006**, *22*, 9860–9865.